C. R. Mecanique 330 (2002) 803–810

Large Eddy Simulation of a plane impinging jet

François Beaubert, Stéphane Viazzo

École des mines de Nantes, GEPEA – UMR CNRS 6144, 4, rue A. Kastler, BP 20722, 44307 Nantes, France

Received 18 June 2002; accepted after revision 26 September 2002

Note presented by Sébastien Candel.

Abstract Large Eddy Simulations of a plane turbulent impinging jet have been carried out using the dynamic Smagorinsky model. The statistical results are first validated with the measurements from the literature: mean and turbulent quantities along the jet axis and at different vertical locations are presented. This study is completed by the analysis of the wall shear stress at the impingement wall. The effect of the jet Reynolds number ($3000 \leqslant Re \leqslant 13500$) on the kinematic development of the jet is also discussed. ***To cite this article: F. Beaubert, S. Viazzo, C. R. Mecanique 330 (2002) 803–810.***

turbulence / large eddy simulation / plane turbulent impinging jet

Simulations des grandes échelles d'un jet plan en impact proche

Résumé Une étude par simulations des grandes échelles turbulentes a été menée sur un jet plan turbulent en impact proche. Les résultats statistiques sont, dans un premier temps, validés par rapport aux mesures de la littérature : les grandeurs moyennes et turbulentes le long de l'axe du jet et à différentes positions verticales sont présentées. Cette étude est complétée par une analyse de la contrainte de cisaillement pariétal. Enfin, l'effet du nombre de Reynolds du jet sur le développement cinématique du jet est également discuté. ***Pour citer cet article : F. Beaubert, S. Viazzo, C. R. Mecanique 330 (2002) 803–810.***

turbulence / simulation des grandes échelles turbulentes / jet plan en impact

Version française abrégée

Si les jets plans turbulents impactants ont été très largement abordés par des techniques expérimentales, ils ont été moins étudiés par des simulations numériques du type DNS ou LES. Les modèles statistiques classiques du type $k-\varepsilon$ ont montré leurs limites actuelles pour ce type de problème (Craft et al. [2]). En revanche, la simulation des grandes échelles turbulentes semble a priori bien adaptée à cette configuration dans la mesure où les grandes échelles fortement énergétiques et anisotropes sont explicitement calculées. Dans ce but, une méthode numérique hermitienne, à pas fractionnaire est utilisée pour résoudre les équations de Navier–Stokes incompressibles. La fermeture des équations filtrées repose sur le concept de viscosité turbulente. En accord avec les travaux de Ribault et al. [4], le modèle de sous-maille de Smagorinsky, initialement mis en oeuvre a révélé son caractère excessivement dissipatif. Ce modèle a été abandonné au profit du modèle de Smagorinsky dynamique (Lilly [9]) apte à traduire les effets locaux d'anisotropie.

E-mail addresses: Francois.Beaubert@emn.fr (F. Beaubert); Stephane.Viazzo@emn.fr (S. Viazzo).

S1631-0721(02)01537-1/FLA

Le domaine de calcul représenté sur la Fig. 1 est une boite rectangulaire de dimensions $H \times L_y \times L_z$. Les directions verticale (Ox) et horizontale (Oy) sont non-homogènes, tandis que la direction transversale (Oz) est homogène. La largeur de la buse de soufflage (centrée sur la frontière supérieure du domaine de calcul) est notée e, le rapport d'ouverture H/e est fixé à 10. Afin de discuter de l'influence du nombre de Reynolds sur le développement cinématique du jet, trois nombres de Reynolds ont été étudiés : $Re = U_0 e/\nu = 3000$, 7500 et 13500. Dans un premier temps, l'évolution de la vitesse moyenne verticale suivant l'axe du jet est confrontée aux mesures de Maurel et Solliec [12] obtenues pour le même rapport H/e et pour $Re = 13500$ et 27000 (cf. Fig. 2). Les résultats sont en bon accord avec l'expérience et montrent qu'au-delà de $Re = 3000$, la longueur du cône potentiel (voisine de $4e$) est indépendante du nombre de Reynolds. L'étude de la demi-largeur du jet b_u montre que celle-ci diminue avec l'augmentation du nombre de Reynolds, les pentes obtenues pour ce rapport d'ouverture étant voisines de celles d'un jet plan libre (cf. Fig. 2). Conformément aux travaux de Tu et Wood [17], le maximum du coefficient de frottement pariétal τ diminue avec l'augmentation du nombre de Reynolds et l'évolution de $\tau/\tau_{\max}$ apparaît être universelle pour $H/e > 7$ et $Re > 6000$ (cf. Fig. 3). Les tensions de Reynolds sont comparées aux mesures de Maurel [12] et un bon accord avec l'expérience est obtenu (cf. Fig. 4). Cette étude montre que pour le rapport d'ouverture considéré ici ($H/e = 10$), le nombre de Reynolds n'influence le développement du jet que pour $3000 < Re < 7500$. Pour des nombres de Reynolds supérieurs le jet semble atteindre un état « asymptotique ».

1. Introduction

If turbulent impinging jets have been the subject of much experimental research work (the vortical structure of the plane impinging jet has been recently investigated by Sakakibara et al. [1]), they have been less studied by numerical simulations like DNS or LES. Classical statistical models like $k-\varepsilon$ have shown their current limits for this flow configuration: overestimation of the potential core, underprediction of the jet expansion, impinging zone poorly described. Craft et al. [2] evaluated the performance of various turbulence models for the plane turbulent impinging jet, but none of the models was able to yield satisfactory results. On the other hand, numerical simulations of the large turbulent scales (LES) seem a priori well adapted to this configuration insofar as the large, strongly energetic and anisotropic eddies are explicitly calculated. Recent Large Eddy Simulations of a free plane turbulent jet have been performed by Dai et al. [3] and Ribault et al. [4]. A few simulations have been performed for the plane turbulent impinging jet, we could quote the works of Hoffmann et Benocci [5], Voke et al. [6] and more recently the study of Cziesla et al. [7]. The purpose of this study is to investigate the ability of Large Eddy Simulation to predict the overall field quantities of the plane turbulent impinging jet including the important impinging region owing a very fine grid. Mean and turbulent quantities along the jet axis and at different vertical locations are presented. The considered configuration being that of an air blast acting like a separator and protector of atmosphere, we have been focused on the behavior of the wall shear stress because of its relevance to heat and mass transfer. Unlike the previous simulations [5–7], in the present work all the LES results are compared to experimental data. The effect of Reynolds number is also discussed.

2. Mathematical formulation

The flow is governed by the three-dimensional time dependent incompressible Navier–Stokes equations which are written in primitive variables. In Large Eddy Simulations, each variable of the flow f is split into a *large anisotropic scale* component $\bar{f}$ (which is computed) and a small scale component f' called *subgrid scale*, which is more isotropic and universal and has to be modeled. This separation is obtained by applying a spatial filter (indicated by an overbar) to the momentum (1) and continuity (2) equations in order

to reduce the amount of spatial scales to be solved. For incompressible flows, the space filtered equations can be written in the following nondimensional form:

$$\frac{\partial \bar{u}_i}{\partial t} + \frac{\partial}{\partial x_j}(\bar{u}_i \bar{u}_j) = -\frac{\partial \overline{P}}{\partial x_i} - \frac{\partial \tau_{ij}}{\partial x_j} + \frac{1}{Re}\frac{\partial^2 \bar{u}_i}{\partial x_j \partial x_j} \tag{1}$$

$$\frac{\partial \bar{u}_i}{\partial x_i} = 0 \tag{2}$$

where the index $i = 1, 2, 3$ refers respectively to the x, y and z directions.

Here, all variables are nondimensionalized by the maximum nozzle exit velocity U_0 on the jet axis and by the nozzle width e. The jet Reynolds number is defined as $Re = U_0 e/\nu$ where ν is the kinematic viscosity. The subgrid scale stress τ_{ij} is expressed using the Leonard decomposition: $\tau_{ij} = \overline{u_i u_j} - \bar{u}_i \bar{u}_j$ and due to the divergence free constraint the pressure is modified according to: $\overline{P} = \overline{p^*} + \frac{1}{3}\tau_{kk}$ with $p^* = p/\rho$.

In the present work, the space filtered equations are closed using a turbulent eddy viscosity hypothesis. The anisotropic part of the subgrid scale stress τ_{ij} is linked to the eddy viscosity ν_τ by the following expression:

$$\tau_{ij} - \frac{\delta_{ij}}{3}\tau_{kk} = -2\nu_\tau \overline{S}_{ij} \quad \text{with } \nu_\tau = C\bar{\Delta}^2 |\overline{S}| \text{ and } |\overline{S}| = \sqrt{2\overline{S}_{ij}\overline{S}_{ij}} \tag{3}$$

where C is the dimensionless model coefficient, $\bar{\Delta} = (\Delta_x \Delta_y \Delta_z)^{1/3}$ the grid filter width and S_{ij} the strain rate tensor.

According to Ribault et al. [4], we have previously found that the subgrid dissipation given by the standard Smagorinsky model is excessively high, resulting in a substantial underprediction of the jet width and an overprediction of the length of the potential core. Furthermore, this model predicts incorrect asymptotic behavior near the walls or in laminar zones. The dynamic Smagorinsky model which overcomes some of the drawbacks of the Smagorinsky model is a suitable alternative. Initially developed by Germano [8] to correct the excessive dissipation of the Smagorinsky model and modified by Lilly [9], this model exhibits the correct asymptotic behavior near the walls and in laminar regions without using delicate non universal wall layers, and does not formally prohibit possible energy backscatter. The constant C which is a priori fixed with the standard Smagorinsky model is thus replaced by a coefficient C_d which is dynamically computed and depends on the local structure of the flow. In order to compute C_d, a test filter denoted by a hat and of width larger than the grid filter is introduced. The model coefficient C_d is a local and instantaneous quantity and thus can vary widely in time and space. However, this desirable property may lead to numerical instabilities caused by negative values of C_d. Accordingly, the model coefficient is averaged in the homogeneous direction. Furthermore, negative values of ν_τ are clipped to zero if the total viscosity $\nu + \nu_\tau$ is negative. The test filter used in the dynamic Smagorinsky model is a symmetric discrete filter based on the trapezoidal rule: $\hat{f}_i = \frac{1}{4}(f_{i-1} + 2f_i + f_{i+1})$. This filter is applied sequentially in each direction. The value of the ratio $\hat{\bar{\Delta}}/\bar{\Delta}$ is fixed to $\sqrt{6}$ (see Najjar and Tafti [10]).

3. Numerical method

The computational domain is a rectangular box of dimensions $H \times L_y \times L_z$. The nozzle width e is centered on the upper boundary of the computational domain (Fig. 1).

According to Schiestel and Viazzo [11] and in order to circumvent the pressure checkerboarding, a staggered MAC mesh is used. The convective terms are considered in the skew-symmetric form since their discrete analogues preserve the global conservation of momentum and kinetic energy on staggered mesh (in the inviscid limit). The spatial discretization is based on fourth order compact schemes in the inhomogeneous vertical (Ox) and horizontal (Oy) directions whereas Fourier pseudo-spectral methods are appropriate in the homogeneous transverse (Oz) direction.

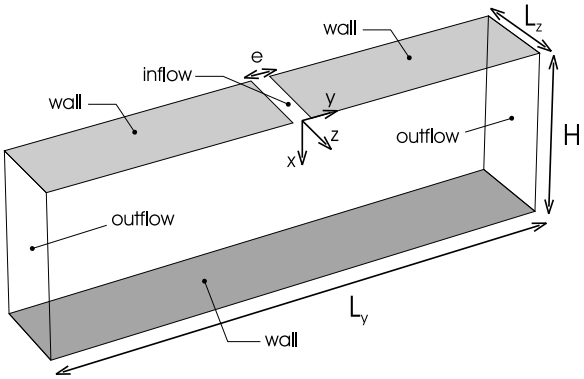

Figure 1. Computational domain.
Figure 1. *Domaine de calcul.*

The time advancement is second order accurate and is based on the explicit Adams–Bashforth scheme for the convective terms and the implicit Crank–Nicolson scheme for the viscous terms. The system of equations is solved using a two-step fractional scheme (*predictor–corrector*). At each time step, the problem reduces to a set of three Helmholtz equations (for the velocity components) and one Poisson equation (for the correction of pressure). The eddy viscosity depends both on time and space, so internal iterations are necessary for solving the predictor step.

At the exit of the jet, a constant (time invariant) inlet vertical velocity profile is used. This profile fits the mean nozzle exit velocity of previous experimental data obtained by Maurel and Solliec [12]. For the outflow regions, a non-reflective convective boundary condition is used to fix each component of the outflow velocity: $\partial u_i/\partial t + V_c \nabla u_i = 0$. The convective velocity V_c is uniform and is deduced from the instantaneous integrated mass flux through the outflow sections. Due to the presence of large vortices at the outflow boundaries, the reentries of fluid may cause an accumulation of instabilities at these locations. In order to prevent numerical instabilities on the outflow boundaries, a buffer domain of extend $5e$ is implemented. A no-slip boundary condition is applied on the walls, whereas Neumann homogeneous conditions are used for the pressure correction. Periodic boundary conditions are appropriate in the homogeneous (Oz) direction.

4. Computational results

The present study is focused on the analysis of statistical quantities (mean and rms quantities) along the jet axis and at different vertical locations. This work is completed by the analysis of the wall shear stress at the impingement wall. The influence of the Reynolds number on the statistical quantities is also presented.

4.1. Computational details

Three different cases are computed to clarify the possible influence of the jet Reynolds number. The Reynolds number $Re = U_0 e/\nu$ is set to 3000 for case (I), 7500 for case (II) and 13500 for case (III). The nondimensional time step $\Delta t U_0/e$ is fixed to a value which ensures the stability of the numerical scheme (CFL < 0.3).

The length of the horizontal direction must be large enough to capture the two large recirculations on each side the jet and to limit the influence of the buffer domain inside the domain of interest. Preliminary bidimensional simulations have been used to assess the influence of the length of the horizontal direction. We concluded that a value of $H_y/e = 40$ is sufficient. In the framework of air curtain applications, the opening ratio H/e is fixed to 10 for all cases. The choice of the length of the homogeneous direction (Oz) is less obvious. Indeed, the periodic boundary conditions along the homogeneous direction are justified only if the transverse dimension H_z is large enough to capture the largest structures of the flow. Consequently, the fluctuations must be practically decorrelated on a half-period ($L_z/2$). Beaubert and Viazzo [13] have

Table 1. Computed cases.

Tableau 1. *Les cas calculés.*

Case	No gridpoints	Δx	Δy	Δz	$\Delta t U_0/e$	Re
I	$160 \times 180 \times 64$	1.11×10^{-2}–0.1232	2.52×10^{-2}–0.74	9.81×10^{-2}	3×10^{-3}	3000
II	$140 \times 240 \times 64$	5.44×10^{-3}–0.1659	$2.40 \times 10^{-2} - 0.90$	9.81×10^{-2}	3×10^{-3}	7500
III	$150 \times 240 \times 64$	$5.44 \times 10^{-3} - 0.1632$	$2.40 \times 10^{-2} - 0.90$	9.81×10^{-2}	1.75×10^{-3}	13500

previously found that a width of 2π for the transverse direction (Oz) is rather advised for the ratio $H/e = 10$ and in this range of Reynolds numbers. The characteristics of the three simulations are summarized in Table 1.

The grid spacing in the (Ox) and (Oy) directions is non-uniform to describe accurately the strong gradient regions with the grid points clustered near the wall and the two mixing layers around the jet axis. The grid is also refined near the detachment point of the wall jets to avoid too large anisotropic grids in these strong gradient regions. We have, as far as possible, maintained an identical distribution of the grid points between the different cases but small adjustments have been necessary with increasing Reynolds number. In the homogeneous (Oz) direction the mesh is uniform.

Long integration times are required in order to ensure the statistical stationarity of the turbulent flow field. The averaging is performed in both time and the transverse homogeneous direction. Once statistical convergence is obtained, the statistics are calculated by averaging over 100 nondimensional time units. For exemple, at $Re = 7500$ first order statistical quantities are roughly established for $TU_0/e = 50$ whereas second order statistics are converged for $TU_0/e = 100$.

4.2. Mean flow and turbulence statistics

In Fig. 2, the centerline $(y/e = 0)$ mean vertical velocity (U_m/U_0) and the jet half width (b_u/e) are reported and a good agreement with the experiment is obtained.

This figure underlines the short length of the potential core (around e) for the smallest Reynolds number (case I). Furthermore, the length of the potential core is Reynolds dependent in the range of 3000 to 7500. Above $Re = 7500$ the length of the potential core reaches a value around $4e$. For $Re = 13500$, the results are in good agreement with the measurements of Maurel and Solliec [12] obtained for the same H/e ratio and for $Re = 13500$ and $Re = 27000$. This trend underlines the fact that the longitudinal evolution of the mean velocity U_m reaches an "asymptotic" state for $Re > 7500$.

For the jet half width b_u/e, a slight dependence on the Reynolds number is observed. For $x/e < 4$, the jet half width seems to be independent of the Reynolds number. This dependence increases with the difference of the slope of the mean vertical velocity profile along the jet axis, which is stronger for $x/e \geqslant 5$. The jet expansion decreases with increasing Reynolds number with smaller differences for the two highest Reynolds numbers. For $x/e > 4$, the evolution of the jet half width is linear. In accordance with the measurements of Namer et Ötügen [14] (obtained for a free jet) the slopes of the lines increase with increasing Reynolds numbers: 0.121 for $Re = 3000$, 0.105 for $Re = 7500$ and 0.093 for $Re = 13500$. This behavior was expected due to the higher turbulence intensity levels obtained for smaller Reynolds numbers (see Fig. 4). For $Re = 7500$, the evolution of the jet half width is closed to the experiments of Browne et al. [15] but for a free turbulent jet at $Re = 7620$. The slopes obtained by the simulations are closed to those obtained for a free turbulent jet: Namer et Ötügen [14] show that the slopes reach an asymptotic value of 0.098 for $Re = 6000$, Browne et al. [15] obtain a slope of 0.104 for $Re = 7620$, value which is very closed to the slope obtained by the the simulation at $Re = 7500$.

The wall shear stress is expressed as a skin friction coefficient defined by: $C_f = 2\,Re^{-1}\,d(V/U_0)/d(x/e) = \tau_w/(0.5\rho U_0^2)$ for $x/e = 10$. For small H/e ratio, the analysis of the Hiemenz solution by Tu [16] leads

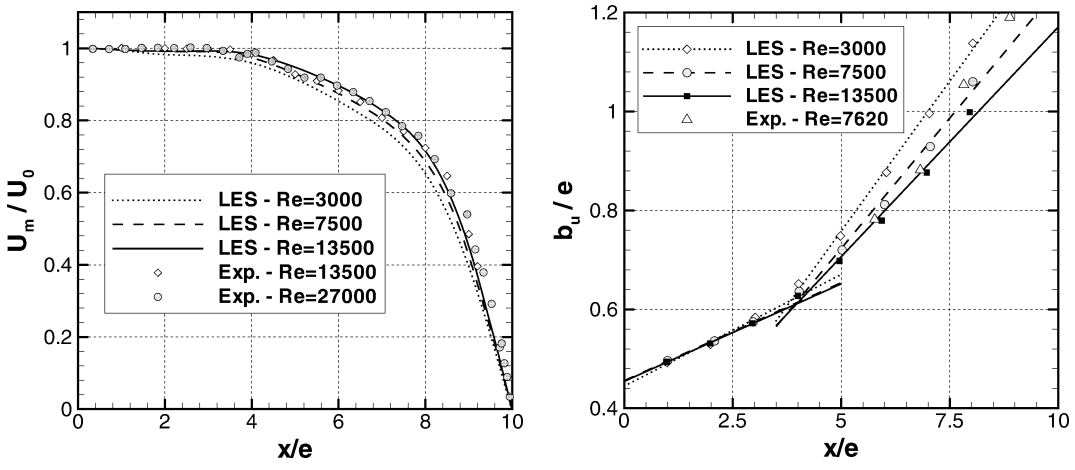

(a) (b)

Figure 2. (a) Mean vertical velocity profiles along the jet axis, Exp. Maurel and Solliec [12]. (b) Evolution of the jet half width b_u, Exp. Browne et al. [15].

Figure 2. (a) *Profils de la vitesse moyenne verticale suivant l'axe du jet, Exp. Maurel et Solliec* [12]. (b) *Evolution de la demi-largeur du jet* b_u*, Exp. Browne et al.* [15].

to the theoretical relation: $\tau_w\sqrt{Re_b}/(0.5\rho U_0^2) = 1.873\xi$ with $Re_b = U_0 b_p/\nu$ and $\xi = y/b_p$ (b_p is the half-width of the impingement pressure: $p(H, b_p) = 0.5p(H, 0)$). The wall shear stress distribution along the impingement wall is shown on Fig. 3. The numerical results (case II and III) are in good agreement with the experiments of Tu and Wood [17] for $H/e = 8$, 12 and $Re = 11000$. The slopes of the computed and measured wall shear stress are significantly smaller than the theoretical ones. For Tu and Wood, the low values may be due to three-dimensional effects related to the existence of streamwise counter-rotating cells in the impingement region which have been also exhibited by the simulations (Beaubert and Viazzo [18]). The discrepancy between experiments at $H/e = 12$ and calculations may be attributed to measurement uncertainties. It is possible that the three-dimensionality of the flow affect the calibration of the probes for large opening ratio H/e. In accordance with Tu and Wood, the maxima of the friction coefficient decrease with increasing Reynolds numbers: 0.012, 0.0086 and 0.0065 respectively for $Re = 3000$, $Re = 7500$ and $Re = 13500$. These values are in very good agreement with the experimental results of Tu and Wood [17] obtained for the same opening ratio ($H/e = 10$) and for $Re = 3040$ and $Re = 6300$. For sufficiently high H/e ratio (> 7 approximately) and Reynolds numbers ($Re > 6000$ approximately), Tu and Wood show that $\tau/\tau_{\max}$ appears to be universal. The present simulations confirm this trend. The distribution of $\tau/\tau_{\max}$ along the impingement wall obtained by the simulations (case II and III) is represented on Fig. 3 and is compared favourably to the measurements of Tu and Wood for $H/e = 8$, 12 and $Re = 11000$.

Fig. 4 shows the distribution of the vertical turbulence intensity $\langle u'^2\rangle^{1/2}$ along the jet axis and the distribution of the Reynolds shear stress $\langle u'v'\rangle$ along the y-direction for different x locations, the numerical results are compared to the measurements of Maurel and Solliec [12] obtained for the same H/e ratio and for $Re = 13500$, 27000. In the development region of the jet, the velocity fluctuations decrease with increasing Reynolds numbers and reach a state independent on Re in the stagnation region. This behavior observed for all the velocity components underlines the fully developed nature of the turbulence in the impinging zone. The peak of turbulence (around 25%) near the impingement ($x/e \simeq 9.5$) is well described by the simulations. This peak is also observed for the other components of the turbulence intensity but closer to the impingement wall. For the horizontal turbulence intensity $\langle v'^2\rangle^{1/2}$, the peak is about two times

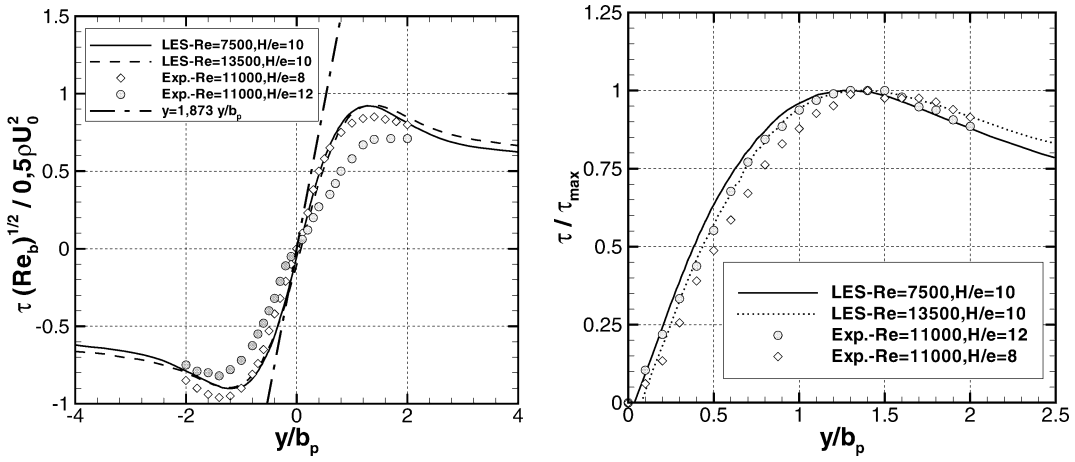

Figure 3. Distribution of the wall shear stress along the impingement wall, Exp. Tu and Wood [17].

Figure 3. *Distribution de la contrainte de cisaillement pariétale sur la paroi d'impact, Exp. Tu et Wood* [17].

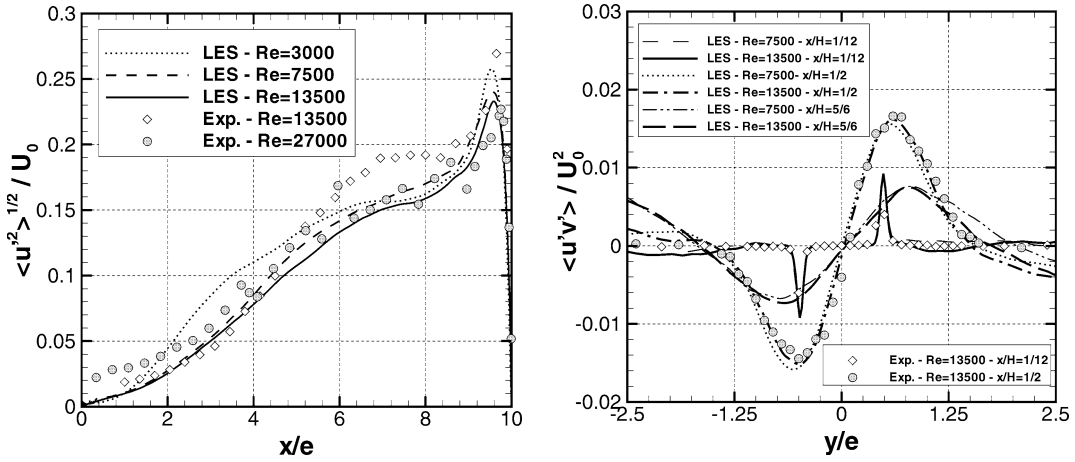

(a) (b)

Figure 4. (a) Vertical distribution of $\langle u'^2\rangle^{1/2}/U_0$ along the jet axis, Exp. Maurel and Solliec [12] – (b) horizontal distribution of $\langle u'v'\rangle/U_0^2$, Exp. [12].

Figure 4. (a) *Distribution verticale de* $\langle u'^2\rangle^{1/2}/U_0$ *le long de l'axe du jet, Exp. Maurel et Solliec* [12] – (b) *distribution horizontale de* $\langle u'v'\rangle/U_0^2$, *Exp.* [12].

smaller than the vertical component, whereas the magnitude of the transverse turbulence intensity $\langle w'^2\rangle^{1/2}$ is of the same order than the $\langle u'^2\rangle^{1/2}$ quantity. The Reynolds shear stress $\langle u'v'\rangle$ distribution along the y-direction are closed to the experiments of Maurel and Solliec [12]. The maxima are located around the shear layer and no Reynolds number effect is significant. These results agree with the fact that small Reynolds number effects are suspected above $Re = 7500$.

5. Conclusions

The present simulations of plane turbulent impinging jets are in good agreement with the experiments and demonstrate the interest of LES in relation to current classical statistical models which are inapropriate for this kind of problem. It was also intended to develop a better understanding of the physics of the plane impinging jet to aid in deriving physically accurate closure models. The statistical analysis reveals the influence of the Reynolds number on the jet structure between 3000 to 7500. Above this value the jet seems to have reached an asymptotic behavior.

Acknowledgements. The calculations were carried out on the NEC-SX5 of the IDRIS center in Paris and at the computer science department of the Ecole des Mines de Nantes. The authors would like to thank R. Schiestel for the numerous and fruitful discussions as well as C. Solliec and S. Maurel for providing experimental results and valuable comments.

References

[1] J. Sakakibara, K. Hishida, W.R.C. Phillips, On the vortical structure in a plane impinging jet, J. Fluid Mech. 434 (2001) 273–300.
[2] T.J. Craft, L.J.W. Graham, B.E. Launder, Impinging jet studies for turbulence model assessment. An examination of the performance of four turbulence models, Int. J. Heat Mass Transfer 36 (1993) 2685–2697.
[3] Y. Dai, T. Kobayashi, N. Taniguchi, Large eddy simulation of plane turbulent jet flow using a new outflow velocity boundary condition, JSME Int. J. 37 (2) (1994) 242–253.
[4] C. Le Ribault, S. Sarkar, S.A. Stanley, Large eddy simulation of a plane jet, Phys. Fluids 11 (10) (1999) 3069–3083.
[5] G. Hoffmann, C. Benocci, Numerical simulation of spatially-developing planar jets, in: 74th Fluid Dynamics Symposium on Application of Direct and Large Eddy Simulation of Transition and Turbulence, Chania, Crete, Greece, 1994, pp. 1–6.
[6] P.R. Voke, S. Gao, D. Leslie, Large-eddy simulations of plane impinging jets, Int. J. Numer. Methods Engrg. 38 (1995) 489–507.
[7] T. Cziesla, G. Biswas, H. Chattopadhyay, N.K. Mitra, Large-eddy simulation of flow and heat transfer in an impinging slot jet, Int. J. Heat Fluid Flow 22 (2001) 500–508.
[8] M. Germano, U. Piomelli, P. Moin, W.H. Cabot, A dynamic subgrid-scale eddy viscosity model, Phys. Fluids A 3 (7) (1991) 1760–1765.
[9] D. Lilly, A proposed modification of the Germano subgrid-scale closure method, Phys. Fluids 4 (3) (1992) 633–635.
[10] F.M. Najjar, D.K. Tafti, Study of discrete test filters and finite difference approximations for the dynamic subgrid-scale stress model, Phys. Fluids 8 (4) (1996) 1076–1088.
[11] R. Schiestel, S. Viazzo, A Hermitian–Fourier numerical method for solving the incompressible Navier–Stokes equations, Computers & Fluids 24 (1995) 739–752.
[12] S. Maurel, C. Solliec, The plane air jet impinging nearby and far from flate plate, Exp. Fluids 31 (6) (2001) 687–697.
[13] F. Beaubert, S. Viazzo, Large eddy simulations of plane turbulent impinging jets, in: 14th Australasian Fluid Mechanics Conference, Adelaide University Australia, 2001, pp. 425–428.
[14] I. Namer, M. Ötugen, Velocity measurements in a plane turbulent air jet at moderate Reynolds numbers, Exp. Fluids 6 (1988) 387–399.
[15] L.W.B. Browne, R.A. Antonia, S. Rajagopalan, A.J. Chambers, Interaction region of a two-dimensional turbulent plane jet in still air, in: R. Dumas, L. Fulachier (Eds.), Structure of Complex Turbulent Shear Flow, 1983.
[16] C.V. Tu, Impingement of Plane Turbulent Jets and their Application in Industrial Coating Control, Ph.D. thesis, Univ. Newcastle, Callaghan, NSW, Australia, 1995.
[17] C.V. Tu, D.H. Wood, Wall pressure and shear stress measurements beneath an impinging jet, Experimental Thermal and Fluid Science 13 (1996) 364–373.
[18] F. Beaubert, S. Viazzo, Large eddy simulations of plane turbulent impinging jets at moderate reynolds numbers, in: 5th International Symposium on Engineering Turbulence Modeling and Measurements, Mallorca, Spain, 2002.